Phys Chem Minerals (2006) 33: 63–71
DOI 10.1007/s00269-005-0055-9

ORIGINAL PAPER

Marco Bruno · Mauro Prencipe · Giovanni Valdre'

Ab initio quantum-mechanical modeling of pyrophyllite [$Al_2Si_4O_{10}(OH)_2$] and talc [$Mg_3Si_4O_{10}(OH)_2$] surfaces

Received: 30 May 2005 / Accepted: 23 November 2005 / Published online: 25 January 2006

Abstract Bulk and slab geometry optimizations and calculations of the electrostatic potential at the surface of both pyrophyllite [$Al_2Si_4O_{10}(OH)_2$] and talc [$Mg_3Si_4O_{10}(OH)_2$] were performed at Hartree–Fock and DFT level. In both pyrophyllite and talc cases, a modest (001) surface relaxation was observed, and the surface preserves the structural features of the crystal: in the case of pyrophyllite the tetrahedral and octahedral sheets are strongly distorted with respect to the ideal hexagonal symmetry (and basal oxygen are located at different heights along the direction normal to the basal plane), whereas the structure of talc deviates slightly from the ideal hexagonal symmetry (almost co-planar basal oxygen). The calculated distortions are fully consistent with those experimentally observed. Although the potentials at the surface of pyrophyllite and talc are of the same order of magnitude, large topological differences were observed, which could possibly be ascribed to the differences between the surface structures of the two minerals. Negative values of the potential are located above the basal oxygen and at the center of the tetrahedral ring; above silicon the potential is always positive. The value of the potential minimum above the center of the tetrahedral ring of pyrophyllite is −0.05 V (at 2 Å from the surface), whereas in the case of talc the minimum is −0.01 V, at 2.7 Å. In the case of pyrophyllite the minimum of potential above the higher basal oxygen is located at 1.1 Å and it has a value of −1.25 V, whereas above the lower oxygen the value of the potential at the minimum is −0.2 V, at 1.25 Å; the talc exhibits a minimum of −0.75 V at 1.2 Å, above the basal oxygen.

M. Bruno · Mauro Prencipe (✉)
Dipartimento di Scienze Mineralogiche e Petrologiche, Università degli Studi di Torino, Via Valperga Caluso 35, 10125 Torino, Italy
E-mail: mauro.prencipe@unito.it
Tel.: +39-011-6705131
Fax: +39-011-2365131

Giovanni Valdre'
Dipartimento di Scienze della Terra e Geologico-Ambientali, Università degli Studi di Bologna, P.zza di Porta S. Donato 1, 40126 Bologna, Italy

Keywords Pyrophyllite · Talc · Quantum-mechanical calculation · Hartree–Fock · Density functional · Electrostatic potential

Introduction

Pyrophyllite ([$Al_2Si_4O_{10}(OH)_2$]; Fig. 1a) and talc ([$Mg_3Si_4O_{10}(OH)_2$]; Fig. 1b) are, respectively, the dioctahedral and trioctahedral terms of the phyllosilicate group consisting of simple 2:1 TOT layers (T stands for the tetrahedral sheet and O for the octahedral one; see for instance, Evans and Guggenheim 1988). The tetrahedral sheet has a Si_2O_5 composition in which individual SiO_4 tetrahedra are linked by sharing three corners (basal oxygen, O^b) with SiO_4 neighbors to form infinite two-dimensional sheets with a hexagonal-based patterns of linked sixfold rings; the plane formed by the basal oxygen is usually named "siloxanic basal plane". The fourth corner (apical oxygen, O^a) does not link to other SiO_4 groups but it is shared with the Al (pyrophyllite) or the Mg (talc) octahedrum. The octahedrally-coordinated cations form a sheet, in which individual polyhedra are laterally linked by edge sharing. In pyrophyllite only 2/3 of the octahedral sites are occupied (Fig. 1a; dioctahedral term), whereas in the talc all three octahedral sites are occupied (Fig. 1b; trioctahedral term). The 2:1 layer is composed of two opposing tetrahedral sheets with the octahedral sheet in between. Since the TOT layer is electrically neutral, no interlayer cations exist in these structures.

Pyrophyllite exists in three polytypic forms: a two layer monoclinic (2 M), a one layer triclinic (1Tc) and a disordered form (Gruner 1934; Zvyagin et al. 1969; Brindley and Wardle 1970). The crystal structure of pyrophyllite-1Tc was determined by Wardle and Brindley (1972) by means of the powder diffraction method and by Lee and Guggenheim (1981) with a single crystal X-ray refinement. Recently, pyrophyllite-1Tc has been studied theoretically by using empirical interatomic potential (Sainz-Diaz et al. 2001) and first-principle quantum mechanical simulations based on

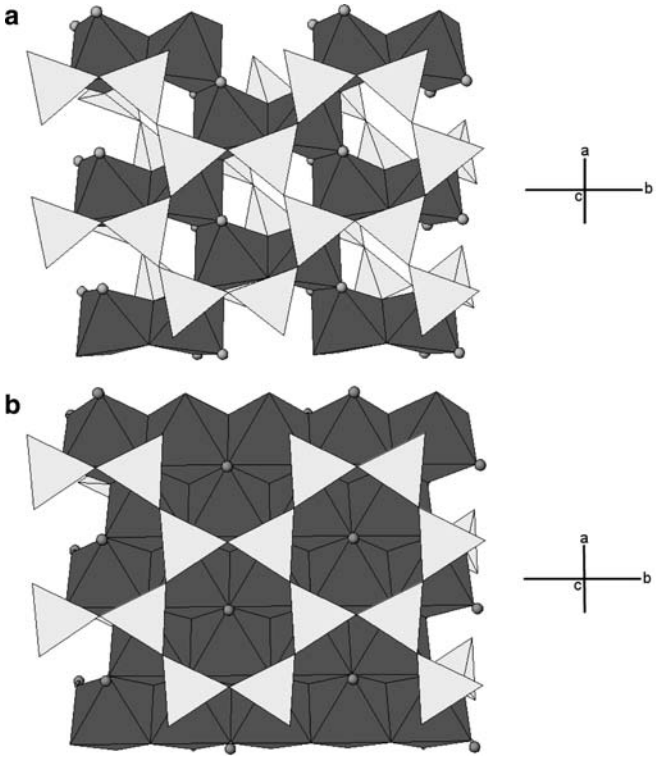

Fig. 1 Pyrophyllite (**a**) and talc (**b**) structures projected along [001]. The *gray sphere* represents the (OH) group

density functional theory (DFT) (Bridgeman et al. 1996; Stackhouse et al. 2001; Refson et al. 2003; Sainz-Diaz et al. 2002, 2004).

Talc has a one layer triclinic structure (1Tc). Rayner and Brown (1973) determined the crystal structure of talc from Weissenberg data, and Perdikatsis and Burzlaff (1981) further refined the structure by X-ray single-crystal diffraction. A quantum mechanical simulation (DFT) of the talc structure has also been performed (Bridgeman et al. 1996).

Bleam (1990) evaluated the electrostatic potential at the siloxanic basal plane [(001) after reorientation of the conventional unit cell, as usually indicated in these systems] of pyrophyllite and talc, by using classical electrostatic, by assigning to the ions the charges derived from an extended Hückel approach (Bleam and Hoffman 1988). For talc, several ab initio or semi empirical calculations on cluster models were performed to determine the electrostatic potential above the surface (Tunega and Turi Nagy 1993; Tunega et al. 1993; Turi Nagy et al. 1996). However, in these works only idealized (001) surface structures were considered. In order to understand the influence of the structural details of the surface on the electrostatic potential, we performed a quantum mechanical study of the (001) surface structure of pyrophyllite-1Tc (space group: $P\bar{1}$) and talc ($P\bar{1}$), whose geometries were optimized at the Hartree–Fock (HF) and DFT level.

The detailed knowledge of the topological distribution of the potential at the surface of talc and pyrophyllite is a first step toward the understanding of surface properties of more complex atomically flat and extended layer silicates surfaces. The present paper reports the first results of a broader research aimed at understanding the surface properties of some layer silicates which are of central importance to clarify the self-assembling, catalytic and polimerization properties of biomolecules such as, DNA, RNA, nucleotides, aminoacids and proteins. In fact, very recent experimental results found layer silicate surfaces responsible for a remarkable variety of DNA and nucleotide adsorption mechanisms and can be used to modulate surface self-assembly and nanopatterning of biomolecules (Valdrè et al. 2004). The ability to control the binding of biomolecules onto non-conductive solid substrates with atomically flat boundaries has very attractive applications in nano-biotechnology, microelectronics, microarrays and sensors (Hansma et al. 1992; Wagner et al. 1994; Wuite 2000; Lyubchenko et al. 2001; Heller 2002). Furthermore, investigating the way in which mineral surfaces interact with biomolecules has fundamental implications considering that these substrates may have played an important role as catalysts in the prebiotic world with important implications for the earth and life sciences (Ferris et al. 1996).

The structure of the paper is as follow: (1) description of basis set, computational parameters and strategy used in the bulk and slab geometry optimizations; (2) presentation of the results, along with their interpretation.

Computational details

Crystal and slab geometry optimizations and calculations of the electrostatic potential at the surface were performed by means of the ab initio CRYSTAL code (Saunders et al. 2003), which implements the Hartree–Fock and Kohn–Sham, self consistent field (SCF) method for the study of periodic systems (Pisani et al. 1988). The graphical representation of the electrostatic potential maps were made by external software (CrGraph2003[1]).

Hamiltonian and computational parameters

The calculations were performed at the HF level, except for a case where a density-functional (DFT) approach was followed. In the latter case, an Hamiltonian (based on the B3LYP scheme; Becke 1993) containing hybrid Hartree–Fock/density-functional exchange-correlation terms was used, which employs the Becke GGA exchange term (B; Becke 1988) mixed with the exact nonlocal HF exchange [in the proportion 0.5 (HF) and 0.5 (B); Prencipe and Nestola 2005], and the Lee–Yang–Parr (LYP; Lee et al. 1988) GGA correlation term.

The exchange-correlation contribution is evaluated numerically by integrating, over the cell volume, a

[1]The Crystal Web page: http://www.crystal.unito.it

function of the electron density and of its gradient. The choice of the grid of points for the integration is based on an atomic partition method, originally developed by Becke (1988). In the present case, the default pruned (55, 434) *p* grid was chosen, which ensures a satisfactory accuracy in geometry optimization.

The thresholds (ITOL1, ITOL2, ITOL3, ITOL4 and ITOL5) controlling the accuracy of the calculation of Coulomb and exchange integrals (Saunders et al. 2003) were set to 10^{-6} (ITOL1 to ITOL4) and 10^{-12} (ITOL5) for all the optimizations.

The diagonalization of the Hamiltonian was performed at 4 **k** points in the reciprocal space (Monkhrost net; Monkhrost and Pack 1976) by setting the shrinking factor IS (Saunders et al. 2003) to 2.

Basis set

The multielectronic wave function is constructed as an antisymmetrized product (Slater determinant) of monoelectronic crystalline orbitals (CO) that are linear combinations of local functions (to be indicated as AO's) centered on each atom of the crystal. In turn, AO's (basis set) are linear combinations of Gaussian-type functions (GTF, the product of a Gaussian times a real solid spherical harmonic to give *s*-, *p*- and *d*-type AO's). In the present case, silicon is described with a 66–21G* basis (Binkley et al. 1980). It consists of six contracted GTF's for the description of both inner *s* and *sp* shells; 2 and 1 functions respectively for the split valence *sp* shell; the symbol * refers to the presence of *d* orbitals. The exponents of the outer *sp* and *d* GTF's have been variationally reoptimized for the present study (0.13 and 0.51 bohr^{-2}, respectively, for both pyrophyllite and talc). For Al, Mg, O, and H, the basis sets 85–11G* (Catti et al. 1994), 8–511G (Harrison and Saunders 1992), 6–21G* (Nada et al. 1990, 1992), and 5–11G (Dovesi et al. 1984) were respectively used. The reoptimized exponents of the outer GTF's for H are 0.341 (talc) and 0.2 bohr^{-2} (pyrophyllite); for O the exponents of the outer *sp* shell are 0.375 (talc) and 0.367 bohr^{-2} (pyrophyllite); whereas the *d* shell exponent is 0.60 bohr^{-2} in both talc and pyrophyllite. The outer *sp* and *d* shells for Al have exponents of 0.54, 0.20 and 0.49 bohr^{-2}, respectively; the exponents of the outer *sp* shells of Mg are 0.66 and 0.14 bohr^{-2}.

Geometry optimization

In the various cases (different Hamiltonian and different basis set), the bulk geometry (fractional coordinates) were optimized starting from the experimental values determined by X-ray diffraction methods (Tables 1, 2, 3; Lee and Guggenheim 1981; Perdikatsis and Burzloff 1981). The optimization of the atomic coordinates was performed by means of a modified conjugate gradient algorithm (Civalleri et al. 2001). Due to limitations in the available computational resources, cell parameters were not optimized and, in all the optimizations, unit cells were kept fixed at the experimental values (Table 1; Lee and Guggenheim 1981; Perdikatsis and Burzloff 1981).

In the case of pyrophyllite, three bulk geometry optimizations were performed: (1) at HF level without *d* orbitals on O (case indicated henceforth with the symbol BH); (2) at HF level with the *d* orbitals on O (BH*), and (3) at DFT level with *d* orbitals on O (BD*). In the case of talc only optimizations BH and BH* were performed; optimizations at DFT level have not been performed since the recourse to a DFT Hamiltonian did not provide significant enhancement in the bulk structure description of pyrophyllite.

For pyrophyllite, mono-, bi- and three-layer slab geometry optimizations were performed without *d* orbitals on O (in the following the three-layer slab optimization is only reported and indicated henceforth with the symbol STL), whereas bi-layer (SBL*; with *d* orbitals on O) slab optimization was performed in the case of talc. Each slab of given thickness was generated by cutting the optimized bulk structure parallel to the (001) plane. All the optimizations of the slab structures were done at HF level.

Electrostatic potential was calculated (starting from the calculated electron density, by using the PROPERTIES program included in the CRYSTAL package, Saunders et al. 2003) at different heights above siloxanic plane, and along directions normal to the surface, for each optimized slab. In order to estimate the effects of the Hamiltonian and of the presence of *d* orbitals on O, in the case of pyrophyllite the potential was evaluated for a bi-layer slab (1) at HF level and with *d* orbitals on O, (2) at HF level without *d* orbitals on O, and (3) at DFT level and with *d* orbitals on O.

Results and discussion

Pyrophyllite bulk

Table 2 lists the fractional coordinates calculated with the bulk optimization BH* and Table 4 lists a set of selected interatomic distances calculated in the different geometry optimizations, together with the experimental distances determined by Lee and Guggenheim (1981).

Bulk optimizations BH, BH* and BD* show that the tetrahedral and octahedral sheets are distorted with respect to the ideal hexagonal symmetry. This implies a rotation of the tetrahedra in the (001) plane (ditrigonal rotation[2] $\alpha = 10.7°$ in BH*) and a decrease of the distances between the apical oxygens (which are the ones

[2]The distorsion (ditrigonal rotation α) is obtained by rotation of the tetrahedra around the perpendicular to the sheet. The angle 2α is defined by the directions of two tetrahedral edges sharing a corner (i. e., Ferraris and Ivaldi 2002; Brigatti and Guggenheim 2002).

Table 1 Experimental cell parameters (*a*, *b* and *c*, in Å): single crystal X-ray data of Lee and Guggenheim (1981) and Perdikatsis and Burzloff (1981) for pyrophyllite and talc, respectively

	a	*b*	*c*	α	β	γ
Pyrophyllite	5.160(2)	9.347(3)	5.186(6)	96.21(4)	120.19(4)	79.54(3)
Talc	5.291(3)	9.460(5)	5.290(3)	98.68(5)	119.90(5)	85.27(5)

Table 2 Experimental (expt = single crystal X-ray data of Lee and Guggenheim 1981) and calculated (BH*; see text for details) fractional coordinates of pyrophyllite

	Expt			BH*		
	x	*y*	*z*	*x*	*y*	*z*
Si(1)	0.2521(2)	0.29169(8)	−0.00606(8)	0.25341	0.29102	−0.00530
Si(2)	−0.4337(2)	0.29230(8)	0.34846(8)	−0.43446	0.29175	−0.34801
Al(1)	−0.3324(2)	−0.00008(9)	0.33410(9)	−0.33220	0.00001	0.33417
O(1)	0.3523(4)	0.1155(2)	0.0036(2)	0.3477	0.1138	0.0022
O(2)	−0.4235(4)	0.1158(2)	−0.3842(2)	−0.4194	0.1143	−0.3811
O(3)	0.3393(4)	0.3589(2)	−0.2218(2)	0.3378	0.3572	−0.2224
O(4)	0.4386(5)	0.3584(2)	0.3274(2)	0.4413	0.3566	0.3285
O(5)	−0.1026(4)	0.3325(2)	−0.1148(2)	−0.1023	0.3312	−0.1106
O(6)	−0.0336(4)	0.1081(2)	0.3854(2)	−0.0338	0.1076	0.3785
H	−0.0426	0.1541	0.2214	−0.0382	0.1197	0.1972

Table 3 Experimental (expt = single crystal X-ray data of Perdikatsis and Burzloff 1981) and calculated (BH*; see text for details) fractional coordinates of talc

	Expt			BH*		
	x	*y*	*z*	*x*	*y*	*z*
Si(1)	0.00518(8)	0.70927(3)	0.25732(7)	0.00513	0.71186	0.25776
Si(2)	0.67140(8)	0.70892(3)	0.58997(7)	0.67178	0.71186	0.59080
Mg(1)	0.00000(0)	0.00000(0)	0.00000(0)	0.00000	0.00000	0.00000
Mg(2)	0.66664(9)	0.00006(4)	0.33320(8)	0.66695	0.00004	0.33384
O(1)	0.6688(2)	0.8824(1)	0.6453(2)	0.6686	0.8850	0.6362
O(2)	0.3348(2)	0.8874(1)	0.9704(2)	0.3354	0.8893	0.9712
O(3)	0.0024(2)	0.8824(1)	0.3032(2)	0.0023	0.8850	0.3035
O(4)	0.8574(2)	0.6519(1)	0.9088(2)	0.8617	0.6546	0.9093
O(5)	0.8218(2)	0.6506(1)	0.3907(2)	0.8189	0.6537	0.3884
O(6)	0.3398(2)	0.6516(1)	0.4270(2)	0.3395	0.6541	0.4308
H	0.338(6)	0.797(2)	0.950(5)	0.334	0.788	0.944

Table 4 Interatomic distances obtained in the pyrophyllite geometry optimizations BH, BH*, BD* and STL (see text for details)

	Bond length (Å)					
	STL		BH	BH*	BD*	Expt
	Layer I–III	Layer II				
Si–O[b]	1.6069	1.6098	1.6050	1.6068	1.6102	1.602(2)
Si–O[b]	1.6091	1.6120	1.6101	1.6108	1.6137	1.615(2)
Si–O[b]	1.6138	1.6135	1.6158	1.6157	1.6197	1.618(2)
Si–O[a]	1.6328	1.6351	1.6315	1.6382	1.6427	1.632(2)
Al–O	1.9140	1.9167	1.9155	1.9292	1.9284	1.926(2)
Al–O	1.9132	1.9160	1.9149	1.9262	1.9247	1.926(2)
Al–O	1.9124	1.9103	1.9146	1.9176	1.9172	1.922(2)
Al–O	1.9122	1.9099	1.9136	1.9160	1.9166	1.922(2)
Al–OH	1.8750	1.8753	1.8758	1.8981	1.8959	1.889(2)
Al–OH	1.8750	1.8728	1.8735	1.8952	1.8936	1.888(2)

Expt single crystal X-ray data of Lee and Guggenheim (1981)
[a] apical oxygen
[b] basal oxygen

shared with Al), as well as a corrugation of the oxygens of the basal plane (the average absolute difference, Δz, in the height between the oxygens amounts to 0.23 Å). Such a deviation from the ideal hexagonal symmetry is consistent with the experimental observations by Lee and Guggenheim (1981) ($\alpha = 10.2°$, $\Delta z = 0.24$ Å) and DFT simulations by Refson et al. (2003) ($\alpha = 10.1°$, $\Delta z = 0.21$ Å). For a detailed discussion on the geometrical parameters describing distortions in layer silicates see, for example, Brigatti and Guggenheim (2002) and references therein.

The experimentally observed difference between the Si–O^a and Si–O^b distances is well reproduced by the calculations. In addition, a fairly good agreement exists between calculated and experimental interatomic distances, the differences being less than 0.6% (Table 4). In particular, as the basis set is concerned (effect of *d* orbitals on O) the Si–O distances obtained in optimizations BH and BH* are not significantly different and match very well the experimental results; in BH and BH*, the Al–O distances show instead small differences, which amount to 0.01 Å on average, with the BH* case being the closest to the experiment. Concerning the Hamiltonian (BH* and BD*), the Si–O distances show a small increase, whereas Al–O ones tend to decrease in passing from the HF Hamiltonian (BH*) to the DFT Hamiltonian (BD*). Interatomic distances obtained with DFT simulations by Refson et al. (2003), which lack a self interaction correction as in our DFT calculations, show average overestimations of the Si–O and Al–O distances which amount to 1.2 and 1.6%, respectively, compared to the experimental results. The same is true for Si–O distances obtained in the DFT simulation by Bridgeman et al. (1996). Such behavior of the calculated M–O distances are in line with the findings of Prencipe and Nestola (2005), concerning the effect of Hamiltonian on the interatomic distances in silicates.

Overall, since the use of *d* orbitals on O or the recourse to a DFT Hamiltonian do not provide significant enhancement in the bulk structure description, in order to achieve the best compromise between accuracy and cost of calculation, we performed slab geometry optimizations at the HF level only, without considering *d* orbitals on O. Nevertheless, in the following the effect of the *d* orbitals and of the DFT Hamiltonian on the electrostatic potential is discussed.

Pyrophyllite slab and electrostatic potential

A three-layer slab geometry optimization (STL) did not produced significantly different results from those obtained in mono- and bi-layer slab optimizations, and interatomic distances in STL are very close to those obtained in BH (bulk optimization; Table 4); this indicates modest (001) surface relaxation; in fact, the ditrigonal rotation α is 11.4° and the Δz of the basal oxygen results to be 0.32 Å.

For such a reason we argue that three layers are sufficient to reproduce bulk-like properties at the center of the slab and to obtain an accurate description of the (001) surface. As a further check of the slab thickness, we computed the electrostatic potential outside the surface and found it to be almost indistinguishable from those computed with one and two-layer slab. Therefore, the three-layer slab was used for the present work to discuss the electrostatic potential generated by the (001) surface.

The topology of the electrostatic potential (V) is clearly shown by the maps presented in Fig. 2a and b. They correspond to the planes parallel to (001) at 1 and 2 Å, respectively, above the average height of the basal oxygens. At 1 Å, a sector with negative electrostatic potential is located in correspondence to lower basal oxygen, whereas sectors with positive potential are above the higher basal oxygen, silicon and approximately at the tetrahedral ring center. At 2 Å, the reverse is observed, except for the positions above the silicon.

Such features are well highlighted by the electrostatic potential curves reported in Fig. 4a, c and d, which were obtained by evaluating V along directions normal to the basal plane for the basal oxygen (Fig. 4a), the tetrahedral ring center (Fig. 4c), and the silicon (Fig. 4d).

The electrostatic potential curve above the higher basal oxygen shows the minimum (−1.25 V) at ∼1.1 Å. Above the lower basal oxygen, the value of the potential at the minimum is −0.2 V, and it is shifted at 1.25 Å. Besides, this curve exhibits a singular trend: it does not decrease in a monotonic way to zero with the increase of the distance from the O, but it shows a positive maximum (0.2 V) at 2 Å. Electrostatic potential curve above the tetrahedral ring center has a very shallow minimum (−0.054 V) at 2 Å. Above silicon the electrostatic potential is always positive.

In order to test the effect of *d* orbitals on O on the electrostatic potential, the latter was determined for a bi-layer slab, by using the 6–21G* basis set for O. The topology of the electrostatic potential and the positions of the minima above lower oxygen, higher oxygen and tetrahedral ring center are almost identical to those previously described, but the values of the potential at the minima differ up to 0.5 V (0.2 V on average) with respect the case without *d* orbitals. As the effect of the Hamiltonian is concerned, small differences in the potential are indeed observed in the proximity of the oxygen atoms; in fact, minima are less pronounced in the DFT case (the average difference of the potential at the minima is 0.15 V), whereas not significant differences are observed at the center of the tetrahedral ring and along the direction for the silicon.

Some differences exist between the electrostatic potential calculated in this work and that reported by Bleam (1990). In particular, values calculated by Bleam (1990) above lower and higher basal oxygen, at $z = 1.86$ Å, are −1.9 and −1.5 V, respectively, which are significantly lower than the values we found at the minima. Furthermore, Bleam (1990) found a local maximum above the silicon atom of −1.1 V, in contrast

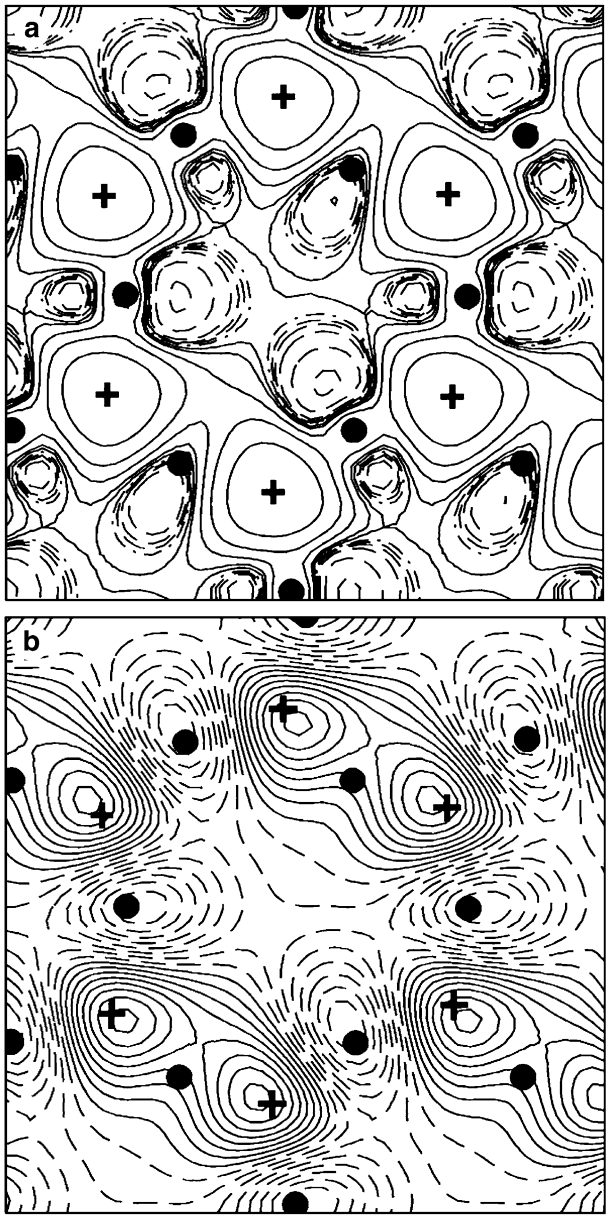

Fig. 2 Electrostatic potential maps at 1 Å (**a**) and 2 Å (**b**) above the (001) surface of the pyrophyllite. *Filled circles* and *crosses* indicate the position of basal oxygen and silicon, respectively. Map covers an area of 7 Å by 7 Å. *Dashed lines* refer to negative values of electrostatic potential. In **a** the minimum value of the potential is -4.57×10^{-2} V, the maximum is 1.70×10^{-1} V; in **b** the minimum and the maximum of the potential are -1.60×10^{-2} V and 1.68×10^{-2} V, respectively

with the positive potential we obtained along the z range investigated.

Talc bulk

Table 3 lists the fractional coordinates calculated with the bulk optimization BH* and Table 5 lists a set of selected interatomic distances calculated with the different geometry optimizations (BH and BH*), together with the experimental distances determined by Perdikatsis and Burzlaff (1981). At variance with the pyrophyllite case, the experimentally geometry is well reproduced (at the same level of pyrophyllite) only in the case of BH* (bulk optimization), but not in BH. Therefore, talc structure can be reasonably described by using the *d* orbitals on O. For this reason, optimization BH is not longer discussed in the following.

Optimizations BH* shows that the tetrahedral and octahedral sheets are only slightly distorted with respect to the ideal hexagonal symmetry: α is 4.2° and Δz of the basal oxygens results to be 0.01 Å. Moreover, the Si–O distances are in good agreement with the experimental ones, whereas the Mg–O distances are slightly smaller (−0.6%). Mg–O bond lengths obtained with DFT simulations by Bridgeman et al. (1996) are overestimated with respect to the experiments by 1.9%, for the reason already discussed in the case of pyrophyllite.

Talc slab and electrostatic potential

Since in the pyrophyllite case the geometry optimization of the three-layer slab did not produce significantly different results with respect to the bi-layer optimization, in the talc case the bi-layer slab (SBL*) only was considered. Moreover, the Si–O and Mg–O distances are very close to those obtained in the bulk optimizations. Thus, as in the case of pyrophyllite, a very modest surface relaxation is observed ($\alpha = 2.3°$ and $\Delta z = 0.005$ Å).

Electrostatic potential was calculated both for a not relaxed three-layer slab (by using fractional coordinates from bulk optimization, BH*, since as said above structural relaxation is expected to be negligible) and for the relaxed bi-layer slab (SBL*); no significant differences between the two cases were observed.

Electrostatic potential maps generated for the three-layer slab above the (001) surface are shown in Fig. 3a, at 1 Å above the surface, and in Fig. 3b, at 2 Å. In both sections, zones with negative electrostatic potential are located above the basal oxygens, whereas zones with positive potential are positioned above the silicon and the tetrahedral ring center. Being the basal oxygen almost co-planar, only one electrostatic potential curve for O is reported (Fig. 4b), which exhibits a minimum of −0.75 V at 1.2 Å.

Electrostatic potential curves calculated in correspondence of silicon and tetrahedral ring center are also reported (Fig. 4c, d). The minimum (−0.013 V) above the tetrahedral ring center is at 2.7 Å, shifted at a higher distance with respect to the minimum calculated for the pyrophyllite. The curve relative to the silicon is very similar to the correspondent in pyrophyllite.

As in the case of pyrophyllite, remarkable differences exist between our results and those reported by Bleam

(1990). Values reported by Bleam (1990) above the basal oxygen atom and at the center of the ring (at 1.86 Å above the surface) are −1.82 and −1.10 V, respectively, which are significantly lower than the values we found at the minima along the z direction; moreover, Bleam (1990) found negative values of the potential above the silicon (−1.11 V, at 1.86 Å above the surface), whereas in our case such potential is always positive.

Very significant differences are observed with respect to the results published by Tunega et al. (1993), which used INDO/2 semi empirical calculations on the cluster model of an idealized mono-layer of talc. The most important feature in their results is a potential which is significantly different from zero at large distances from the surface. They claim that the mean potential approaches to zero at about 50 nm, whereas in our case the potential is essentially zero at distances higher than 1 nm, in agreement with the finding of Bleam (1990).

Conclusion

Bulk and slab geometry optimizations of both pyrophyllite and talc were performed at HF and DFT level, and the potential at the (001) surface was evaluated; in both cases, the interatomic distances in slab optimizations were very close to those obtained in bulk optimizations; this indicates modest (001) surface relaxation. In the case of pyrophyllite the tetrahedral and octahedral sheets are distorted with respect to the ideal hexagonal symmetry, the tetrahedra being rotated ($\alpha = 11.4°$) and tilted in the (001) plane; this implies a corrugation of the basal plane, with the basal oxygens located at different heights along the direction normal to (001) ($\Delta z = 0.32$ Å). In the case of talc the tetrahedral and octahedral sheets are only slightly distorted with respect to the ideal hexagonal symmetry, and the basal oxygens are almost co-planar ($\alpha = 2.3°$ and $\Delta z = 0.005$ Å).

Although the potentials at the surface of pyrophyllite and talc are of the same order of magnitude, large topological differences were observed, which could possibly be ascribed to the differences between the surface structures of the two minerals. The strong deviation from the ideal hexagonal symmetry, in particular the corrugation of the surface caused by the tetrahedral tilting, is a peculiarity of the dioctahedral 2:1 TOT layer silicates (Ferraris and Ivaldi 2002). Indeed, structural distortions are particularly marked in muscovite [dioctahedral; $KAl_2AlSi_3O_{10}(OH)_2$], whereas phlogopite [trioctahedral; $KMg_3AlSi_3O_{10}(OH)_2$] is only slightly affected by these modifications. The deviation from the ideal hexagonal symmetry in mica structures is due to the dimensions of the T and of the O sheets which do not match; therefore, some structural distortions are needed, particularly in the case of dioctahedral micas, where the T–O mismatch is larger with respect to that in the trioctahedral micas (Ferraris and Ivaldi 2002).

Such large differences in the topology of the potential at siloxanic surface of pyrophyllite and talc could be related to some experimental observations (Valdrè et al. 2004), which show that the basal planes of trioctahedral 2:1 TOT layer silicates (biotite, phlogopite, talc) and brucite have a much higher affinity for DNA with respect to the basal plane of a dioctahedral mica like muscovite. The experiments were conducted by observing at a nanoscale level the interaction of freshly cleaved

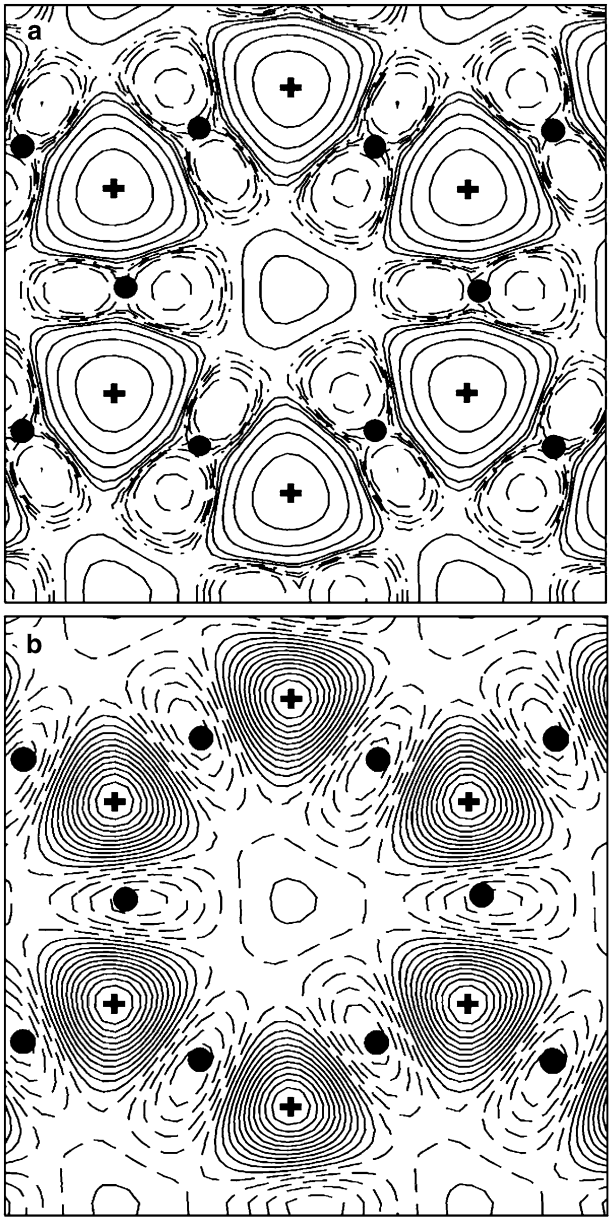

Fig. 3 Electrostatic potential maps at 1 Å (**a**) and 2 Å (**b**) above the (001) surface of the talc. *Filled circles* and *crosses* indicate the position of basal oxygen and silicon, respectively. Map covers an area of 7 Å by 7 Å. *Dashed lines* refer to negative values of electrostatic potential. In **a** the minimum value of the potential is -2.67×10^{-2} V, the maximum is 1.35×10^{-1} V; in **b** the minimum and the maximum of the potential are -5.94×10^{-3} V and 1.14×10^{-2} V, respectively

Table 5 Interatomic distances obtained in the talc geometry optimizations BH, BH* and SBL* (see text for details)

	Bond length (Å)			
	SBL*	BH	BH*	Expt
Si–O[b]	1.6233	1.6131	1.6233	1.625
Si–O[b]	1.6231	1.6137	1.6244	1.624
Si–O[b]	1.6227	1.6151	1.6258	1.623
Si–O[a]	1.6175	1.6286	1.6189	1.612
Mg–O	2.0660	2.0757	2.0667	2.080
Mg–O	2.0640	2.0744	2.0661	2.079
Mg–O	2.0636	2.0733	2.0648	2.078
Mg–O	2.0626	2.0713	2.0623	2.076
Mg–OH	2.0488	2.0555	2.0486	2.058
Mg–OH	2.0475	2.0542	2.0466	2.053

Expt single crystal X-ray data of Perdikatsis and Burzloff (1981)
[a] apical oxygen
[b] basal oxygen

surfaces of layer minerals with aqueous solution containing 5 mM DNA and 10 mM $MgCl_2$. The percentage of area coated by DNA is resulted to be 40, 58 and 2%, for biotite, brucite and muscovite, respectively (Valdrè et al. 2004).

A possible explanation is that the high affinity for DNA of the trioctahedral layer silicates and brucite is a consequence of the small distortion from the ideal hexagonal symmetry of their (001) surface. By contrast, the remarkable distortion of the tetrahedral and octahedral

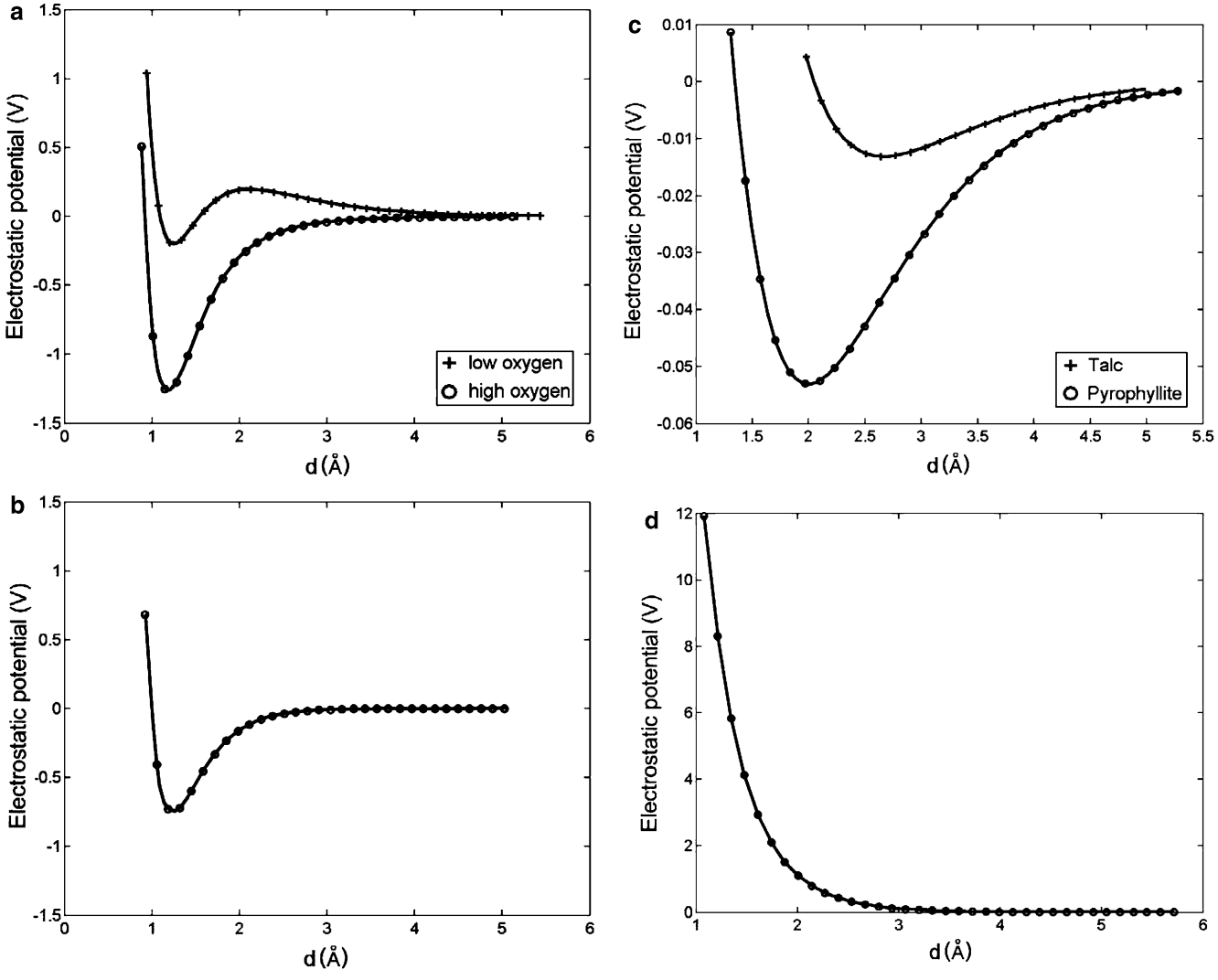

Fig. 4 Electrostatic potential versus distance calculated above the basal oxygen of pyrophyllite (**a**) and talc (**b**), above the center of the tetrahedral ring (**c**) and the silicon (**d**) of both pyrophyllite and talc

sheets in the dioctahedral micas seems to hinder the binding of DNA onto the basal plane of these minerals. However, in order to verify this hypothesis a systematic study of other types of layered minerals is needed.

References

Becke AD (1988) Density-functional exchange-energy approximation with correct asymptotic behaviour. Phys Rev A38:3098–3100

Becke AD (1993) Density functional thermochemistry.3. The role of exact exchange. J Chem Phys 98:5648–5652

Binkley JS, Pople JA, Hehre WJ (1980) Self-consistent molecular orbital methods. 21. Small split-valence basis sets for first-row elements. J Am Chem Soc 102:939–947

Bleam WF (1990) Electrostatic potential at the basal (001) surface of talc and pyrophyllite as related to tetrahedral sheet distortions. Clay Clay Miner 38:522–526

Bleam WF, Hoffmann R (1988) Orbital interactions in phyllosilicates: perturbations of an idealized two-dimensional, infinite silicate frame. Phys Chem Miner 15:398–408

Bridgeman CH, Buckingham AD, Skipper NT, Payne MC (1996) Ab-initio total energy study of uncharged 2:1 clays and their interaction with water. Mol Phys 89:879–888

Brigatti MF, Guggenheim S (2002) Mica crystal chemistry and the influence of pressure, temperature, and solid solution on atomistic models. In: Mottana A, Sassi PF, Thompson JB, Guggenheim S (eds) Micas: crystal chemistry and metamorphic petrology, vol 46. Reviews in Mineralogy and Geochemistry, Mineralogical Society of America, Washington, D.C. pp 1–98

Brindley GW, Wardle R (1970) Monoclinic and triclinic forms of pyrophyllite and pyrophyllite anhydride. Am Miner 55:1259–1272

Catti M, Valerio G, Dovesi R, Causà M (1994) Quantum-mechanical calculations of the solid-state equilibrium MgO + α - Al_2O_3↔ $MgAl_2O_4$ (spinel) versus pressure. Phys Rev (B) 49:14179–14187

Civalleri B, D'Arco Ph, Orlando R, Saunders VR, Dovesi R (2001) Hartree-Fock geometry optimisation of periodic systems with the CRYSTAL code. Chem Phys Lett 348:131–138

Dovesi R, Ermondi E, Ferrero E, Pisani, Roetti C (1984) Hartree-Fock study of lithium hydride with a polarizable basis set. Phys Rev (B) 29:3591–3600

Evans BW, Guggenheim S (1988) Talc, pyrophyllite, and related minerals. In: Bailey SW (ed) Hydrous phyllosilicates, vol 19. Reviews in Mineralogy, Mineralogical Society of America, Washington, D.C. pp 225–294

Ferraris G, Ivaldi G (2002) Structural features of micas. In: Mottana A, Sassi PF, Thompson JB, Guggenheim S (eds) Micas: crystal chemistry and metamorphic petrology, vol 46. Reviews in Mineralogy and Geochemistry, Mineralogical Society of America, Washington, D.C. pp 117–153

Ferris JP, Hill AR Jr, Liu R, Orgel LE (1996) Synthesis of long prebiotic oligomers on minerals surfaces. Nature 381:59–61

Gruner JW (1934) The crystal structures of talc and pyrophyllite. Z Kristallogr 55:412–419

Hansma HG, Vesenka J, Siegerist C, Kelderman G, Morrett H, Sinsheimer RL, Elings V, Bustamante C, Hansma PK (1992) Reproducible imaging and dissection of plasmid DNA under liquid with the atomic force microscope. Science 256:1180–1184

Harrison NM, Saunders VR (1992) The structural properties of beta-$MgCl_2$: an ab initio study. J Phys Cond Matter 4:3873–3882

Heller MJ (2002) DNA microarray technology: devices, systems, and applications. Ann Rev Biomed Eng 4:129–153

Lee JH, Guggenheim S (1981) Single crystal X-ray refinement of pyrophyllite-1Tc. Am Miner 66:350–357

Lee C, Yang W, Parr RG (1988) Development of the Colle–Salvetti correlation-energy formula into a functional of the electron density. Phys Rev B37:785–789

Lyubchenko YL, Glall A, Shlyakhtenko L (2001) DNA–protein Interactions: Principles and Protocols, In: Moss T (ed) Laval University, Quebec, Canada, p 656

Monkhrost HJ, Pack JD (1976) Special points for Brillouin-zone integration. Phys Rev B8:5188–5192

Nada R, Catlow CRA, Dovesi R, Pisani C (1990) An ab-initio Hartree–Fock study of α-quartz and stishovite. Phys Chem Miner 17:353–362

Nada R, Catlow CRA, Dovesi R, Saunders VR (1992) An ab-initio Hartree–Fock study of the ilmenite-structured $MgSiO_3$. Proc R Soc Lond A 436:499–509

Perdikatsis B, Burzlaff H (1981) Strukturverfeinerung am talk $Mg_3[(OH)_2Si_4O_{10}]$. Z Kristallogr 156:177–186

Pisani C, Dovesi R, Roetti C (1988) Hartree–Fock ab-initio treatment of crystalline systems. Lecture Notes in Chemistry, 48 Springer, Berlin, Heidelberg, New York

Prencipe M, Nestola F (2005) Ab initio quantum-mechanical modeling of minerals at high pressure. The role of the Hamiltonian in a case study: the beryl ($Al_4Be_6Si_{12}O_{36}$). Phys Chem Miner DOI: 10.1007/s00269-005-0024-3

Rayner JH, Brown G (1973) The crystal structure of talc. Clay Clay Miner 21:103–114

Refson K, Park SH, Sposito G (2003) Ab initio computational crystallography of 2:1 clay minerals. 1. Pyrophyllite-1Tc. J Phys Chem B 107:13376–13383

Sainz-Díaz CI, Hernández-Laguna A, Dove MT (2001) Modelling of dioctahedral 2:1 phyllosilicates by means of transferable empirical potentials. Phys Chem Miner 28:130–141

Sainz-Díaz CI, Timòn V, Botella V, Artacho E, Hernández-Laguna A (2002) Quantum mechanical calculations of dioctahedral 2:1 phyllosilicates: effect of octahedral cation distributions in pyrophyllite, illite and smectite. Am Miner 87:958–965

Sainz-Díaz CI, Escamilla-Roa E, Hernández-Laguna A (2004) Pyrophyllite dehydroxylation process by first principles calculations. Am Miner 89:1092–1100

Saunders VR, Dovesi R, Roetti C, Orlando R, Zicovich-Wilson CM, Harrison NM, Doll K, Civalleri B, Bush LJ, D'Arco Ph, Llunell M (2003) CRYSTAL2003 user's manual. University of Torino, Torino

Stackhouse S, Coveney PV, Sandre E (2001) Plane-wave density functional theoretic study of formation of clay-polymer nanocomposite materials by self-catalyzed in situ intercalative polymerization. J Am Chem Soc 123:11764–11774

Tunega D, Turi Nagy L (1993) Calculation of electron structure of talc by semiempirical methods of quantum chemistry. Ceramics 37:145–147

Tunega D, Turi Nagy L, Varga Š (1993) Semiempirical quantum-chemical calculation of electrostatic potential generated by idealized layer of talc. Chem Papers 47:273–278

Turi Nagy LT, Tunega D, Liška M (1996) Modeling of interaction properties of surfaces of phyllosilicates: a theoretical forecast of adsorption isotherms of noble gases at the talc surface. Int J Quantum Chem 57:843–849

Valdrè G, Antognozzi M, Wotherspoon A, Miles MJ (2004) Influence of properties of layered silicate minerals on adsorbed DNA surface affinity, self-assembly and nanopatterning. Philos Mag Lett 28:539–545

Wagner P, Kernen P, Ungewickell E, Semenza G (1994) Covalent anchoring of proteins onto gold-directed Nhs-terminated self-assembled monolayers in aqueous buffers-Sfm Images of Clathrin Cages and Triskelia. FEBS Lett 356:267–271

Wardle R, Brindley GW (1972) The crystal structures of pyrophyllite-1Tc, and of its dehydroxylate. Am Miner 57:732–750

Wuite GJL, Smith SB, Young M, Keller D, Bustamante C (2000) Single-molecule studies of the effect of template tension on T7 DNA polymerase activity. Nature 404:103–106

Zvyagin BB, Mishchenko KS, Soboleva SV (1969) Structures of pyrophyllite and talc in relation to the polytypes of mica-type minerals. Sov Phys Crystallogr 13:511–515